

Real space imaging of the metal - insulator phase separation in the band width controlled organic Mott system κ -(BEDT-TTF)₂Cu[N(CN)₂]Br

T. Sasaki, N. Yoneyama, and N. Kobayashi

Institute for Materials Research, Tohoku University, Katahira 2-1-1, Sendai 980-8577, Japan

Y. Ikemoto and H. Kimura

SPRING-8, Japan Science Radiation Research Institute, Mikazuki, Hyogo 679-5198, Japan

(Dated: May 23, 2019)

Systematic investigation of the electronic phase separation on macroscopic scale is reported in the organic Mott system κ -(BEDT-TTF)₂Cu[N(CN)₂]Br. Real space imaging of the phase separation is obtained by means of scanning micro-region infrared spectroscopy using the synchrotron radiation. The phase separation appears near the Mott boundary and changes its metal-insulator fraction with the substitution ratio x in κ -[(*h*-BEDT-TTF)_{1-x}(*d*-BEDT-TTF)_{*x*}]₂Cu[N(CN)₂]Br, which band width is controlled by the substitution ratio x between the hydrated BEDT-TTF molecule (*h*-BEDT-TTF) and the deuterated one (*d*-BEDT-TTF). The phase separation phenomenon observed in this class of organics is considered on the basis of the strongly correlated electronic phase diagram and the order-disorder glass transition of the terminal ethylene groups in BEDT-TTF molecules.

PACS numbers: 74.70.Kn, 78.30.Jw, 71.30.+h

I. INTRODUCTION

Microscopic spatially inhomogeneous electronic states have attracted much attention recently in many kinds of correlated electron systems. These electronic inhomogeneities have been considered not to be a heterogeneous mixture consisting of the multiphases with different chemical compositions such as the phase separation in the metal alloys. The materials with such intrinsic electronic inhomogeneity tend to possess a criticality of changes in charge, spin, orbital, and lattice degrees of freedom in the correlated electrons. Various types of the space conformation of the inhomogeneity and the response to the bulk properties have been found. Nano-scale spatial variation of the superconducting gap has been revealed in the superconducting state of Bi₂Sr₂CaCu₂O_{8+δ} by the scanning tunnelling spectroscopy and microscopy¹. In the normal state, charge carriers doped into antiferromagnetic insulators tend to group into some regions of the sample in the form of stripes in some copper oxides². Meanwhile a different kind of the microscopic phase separation takes place in half-doped manganese oxides³. Small variation from half doping causes phase segregation of electron-rich ferromagnetic and electron-poor antiferromagnetic domains with submicron size within the charge ordered phase. In the system with Mott transition, the nano-scale electronic inhomogeneity with preferred orientation has been found in slightly doped Mott insulator Ca_{2-x}Na_xCuO₂Cl₂^{4,5}.

Organic charge transfer salts based on the donor molecule bis(ethylenedithio)tetrathiafulvalene, abbreviated BEDT-TTF or ET, have been recognized as one of the highly correlated electron system⁶. Among them, κ -(BEDT-TTF)₂X with X = Cu(NCS)₂, Cu[N(CN)₂]Y (Y = Br and Cl), etc. have attracted considerable attention from the point of view of the strongly correlated

quasi two dimensional electron system because the strong dimer structure consisting of two BEDT-TTF molecules makes the conduction band effectively half-filling^{7,8,9}. In such a strongly correlated electronic system, several electronic phases appear and the transitions among these phases are controlled by the applied pressure^{10,11} and slight chemical substitution of the donor¹² and anion molecules¹³, which must change the conduction band width W with respect to the effective Coulomb repulsion U_{dimer} between two electrons on a dimer^{7,8,14}. The Mott first order metal - insulator transition divides the superconducting and antiferromagnetic (AF) Mott insulator phases. The Mott transition line is extended to higher temperature beyond the superconducting transition temperature T_c and AF Mott transition temperature T_N and terminated at the critical end point $T_{\text{cr}} \simeq 40$ K^{10,15,16,17}. From T_{cr} to both weak and strong correlation sides in the phase diagram, the T^* line and the bad metal - insulator line T_{ins} are elongated^{18,19,20}. In temperature above T_{cr} , T^* , and T_{ins} , the half-filling bad metallic state exists in wide range of the correlation strength which can be tuned by pressure and substitution of anion. In the weak correlation side from T_{cr} , the bad metal changes to a correlated good metal through T^* and then becomes superconducting. In the strong correlation side, the bad metal develops into a Mott insulator through T_{ins} and then becomes AF Mott insulator at T_N . Thus the κ -(BEDT-TTF)₂X family has been considered to be the band width controlled Mott system in comparison to the filling controlled one in the inorganic perovskites such as High- T_c copper oxides.

In addition to such the strong electronic correlation, characteristic flexibility in the molecules and the crystal lattices plays an important role cooperatively for modulating the electronic properties in κ -(BEDT-TTF)₂X. Particularly the terminal ethylene groups of BEDT-TTF molecules have conformational order-disorder glass tran-

sition at $T_g \simeq 80$ K^{20,21}. The degree of the disorder changes with the cooling speed at T_g . Faster cooling induces a large number of disorders in the terminal ethylene groups at low temperatures. This kind of disorders on molecular scale has been found to be concerned with the pinning effect of vortices²² and the quasiparticle scattering²³. Moreover the slight internal chemical pressure induced by such disorders can switch the ground states in the samples located very near the Mott transition²⁴.

Inhomogeneous electronic states have been suggested in the ¹³C-NMR experiments near the first order metal-insulator transition in the artificially band width controlled κ -(BEDT-TTF)₂Cu[N(CN)₂]Br²⁵. Below characteristic temperature T^* , ¹³C-NMR lines fall into two groups indicating the metallic and antiferromagnetic insulating nature. The results imply that two phases coexist spatially and statically. Subsequent transport experiments have suggested also such the coexistence of two phases at low temperature²⁶. Recently the real space imaging of the inhomogeneous electronic states has revealed the existence of the phase separation of the metal and insulator regions on micrometer scale near the Mott transition of the band width controlled κ -(BEDT-TTF)₂Cu[N(CN)₂]Br²⁷. Although it has been demonstrated that the phase separation phenomenon is realized near the Mott transition, the detail of the morphology, spatial distribution, size of domains and stability of the inhomogeneity have not been clarified yet. It is very important to obtain the detail of the real space information which can give us a clue to know the mechanism of the macroscopic phase separation observed in the strongly correlated electronic system.

In this paper we present the detail of the real space imaging of the electronic phase separation in the organic Mott system κ -[(*h*-ET)_{1-*x*}(*d*-ET)_{*x*}]₂Cu[N(CN)₂]Br, which band width is controlled by the substitution ratio *x* between the hydrated BEDT-TTF molecule (*h*-BEDT-TTF or *h*-ET) and the deuterated one (*d*-BEDT-TTF or *d*-ET).@ Scanning micro region infrared reflectance spectroscopy using the synchrotron radiation is applied to perform the two dimensional imaging of the local electronic state. A part of the present study has been reported recently as the letter form²⁷. This is subsequent paper which contains the comprehensive results on the wide substitution *x* dependence and the cooling condition dependence. On the basis of these results, the origin of the phase separation on macroscopic scale is discussed from the point of view of the electronic phase diagram and the characteristic order-disorder glass transition of the terminal ethylene groups of BEDT-TTF molecules.

II. EXPERIMENTS

Single crystals of κ -[(*h*-ET)_{1-*x*}(*d*-ET)_{*x*}]₂Cu[N(CN)₂]Br partly substituted by deuterated

BEDT-TTF molecule were grown by the standard electrochemical oxidation method²⁸. The typical dimensions of the samples obtained were $\sim 1 \times 1 \times 0.2$ mm³. The largest rhombic surface corresponds to the conducting *c*-*a* plane. The substitution ratio *x* denotes the nominal mole ratio to the fully deuterated BEDT-TTF molecule in the crystallization. We checked the actual substitution with respect to the nominal value *x* by measuring the intensity of the molecular vibrational mode of the terminal ethylene groups. The substitution dependence of the macroscopic phase diagram and the superconducting properties have been examined²⁸. The full volume of the superconductivity has been observed in the range of *x* = 0 – 0.5 when the samples are cooled slowly. In this substitution range, T_c is increased slightly by about 0.1 K with *x* up to ~ 0.1 . Then T_c is kept at constant value of 11.9 K with *x* up to ~ 0.5 . Above *x* = 0.5, however, the superconducting volume fraction decreases and becomes about a few ten vol% at *x* = 1, which value strongly depends on the cooling condition. Concurrently with the reduction of the superconducting volume fraction, T_c starts to decrease from 11.9 K in *x* = 0.5 to 11.6 K in *x* = 1. The rest of the superconducting part may be the AF Mott insulator, and then magnetic impurity effect coming from such the coexistence may reduce T_c . This simple substitution makes it possible to control the band width continuously at ambient pressure with minimal disorder effect. In quick cooling, however, both the superconducting volume fraction and T_c decreases considerably with *x*. This superconducting volume fraction deduced from the magnetization measurements will be shown in Fig. 4 together with the results in the present paper.

Scanning micro region infrared reflectance spectroscopy (SMIS) measurements using the synchrotron radiation (SR) were performed at BL43IR in SPring-8^{29,30}. The polarized reflectance spectra were measured on the *c*-*a* plane along *E* \parallel *a*-axis and *E* \parallel *c*-axis with a Fourier transform spectrometer (Bruker, 120HR/X) using KBr beam splitter and a polarizer in the mid-infrared (IR) range by use of a mercury-cadmium-telluride detector at 77 K. An IR microscope with the controlled precision *x*-*y* stage and high brilliance of SR light enable us to obtain the two dimensional reflectance spectrum map with the spatial resolution of ~ 10 μ m with no apertures²⁹. The sample was fixed by the conductive carbon paste on the sample holder with a gold mirror which was placed at the cold head of the helium flow type refrigerator. The window of the cryostat was BaF₂. We gave careful consideration of less stress and good thermal contact to the crystals in the sample setting. In the normal cooling condition, the samples were cooled slowly from room temperature to 4 K in the rate of about 0.4 K/min. Other conditions in the rapid cool and thermal cycle experiments will be mentioned at the corresponding part in the text. The reflectivity was obtained by comparison to the gold mirror at each temperature measured. It took about one minute to acquire the IR spectrum at each

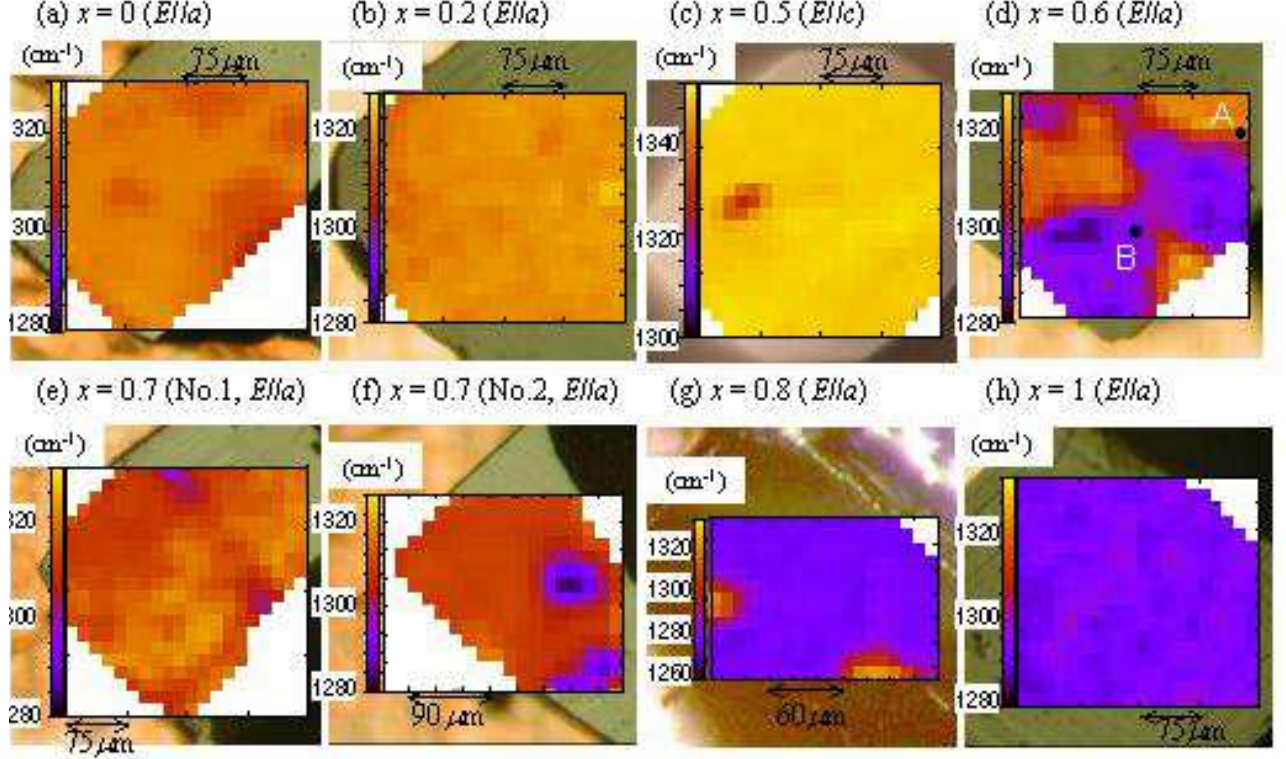


FIG. 1: (Color online) Two dimensional contour map of the peak frequency of the $\nu_3(a_g)$ mode on the crystal surface of $\kappa\text{-}[(h\text{-ET})_{1-x}(d\text{-ET})_x]_2\text{Cu}[\text{N}(\text{CN})_2]\text{Br}$ in (a) $x = 0$ ($E \parallel a$), (b) $x = 0.2$ ($E \parallel a$), (c) $x = 0.5$ ($E \parallel c$), (d) $x = 0.6$ ($E \parallel a$), (e) $x = 0.7$ No.1 ($E \parallel a$), (f) $x = 0.7$ No. 2 ($E \parallel a$), (g) $x = 0.8$ ($E \parallel a$) and (h) $x = 1$ ($E \parallel a$) at 4 K. Bright color (higher frequency) indicates the metallic nature and dark color (lower frequency) does the insulating one. Spectra taken at the points A (metallic region) and B (insulating region) in Fig.1(d) are shown in Figs. 2(a) and 2(b), respectively

scanning point in the case of the spectral resolution of 2 cm^{-1} and accumulation of 100 times. Thus the total measurement time was about 8 hours for obtaining one imaging map ($\sim 0.3 \times 0.3 \text{ mm}^2$).@

III. RESULTS AND DISCUSSION

In order to make the real space image of the electronic states on the crystal surface by SMIS measurements, we use the shift of the frequency ω_3 of a molecular vibration mode $\nu_3(a_g)$. The specific $\nu_3(a_g)$ mode, which is a symmetric stretching mode of the central double bonded carbon atoms of BEDT-TTF molecule, has been found to be very sensitive to difference between metallic and insulating states¹⁹ due to the large electron-molecular vibration coupling^{31,32}. The peak of the $\nu_3(a_g)$ mode should shift to lower frequency in sharper shape in the insulating state at low temperature, while it shows opposite feature in the metallic state. We have obtained the real space imaging of the electronic phase separation in the $x = 0.5$ and 0.8 samples of $\kappa\text{-}[(h\text{-ET})_{1-x}(d\text{-ET})_x]_2\text{Cu}[\text{N}(\text{CN})_2]\text{Br}$ by using such IR frequency shift of the $\nu_3(a_g)$ mode²⁷.

Figure 1 shows the two dimensional contour maps of

the reflectivity peak frequency ω_3 of $\nu_3(a_g)$ mode at 4 K in (a) $x = 0$ ($E \parallel a$), (b) $x = 0.2$ ($E \parallel a$), (c) $x = 0.5$ ($E \parallel c$), (d) $x = 0.6$ ($E \parallel a$), (e) $x = 0.7$ No.1 ($E \parallel a$), (f) $x = 0.7$ No. 2 ($E \parallel a$), (g) $x = 0.8$ ($E \parallel a$), and (h) $x = 1$ ($E \parallel a$). In the contour maps, bright region indicates the higher frequency of ω_3 which demonstrates the metallic feature. It is noted here that higher frequencies of ω_3 observed in the metallic (or insulating) region of $x = 0.5$ samples ($E \parallel c$) in comparison to those of the other samples ($E \parallel a$) are caused by the polarization dependence of the $\nu_3(a_g)$ mode¹⁹. Considering the experimental temperature of 4 K, the metallic region should be superconducting, which has been suggested by the bulk magnetization measurements²⁸. We cite, however, a metal instead of a superconductivity in the higher frequency region at 4 K because it is difficult to distinguish between two states in the present experimental method.

In the samples with small substitution ratio of $x = 0$ and 0.2 , the almost homogeneous metallic state is realized in their whole area. Contrary to this, the sample of the opposite end member $x = 1$ shows the homogeneous insulating state. In the intermediate substitution, however, inhomogeneous features on a micrometer scale can be seen in the maps. The insulating domains appear on

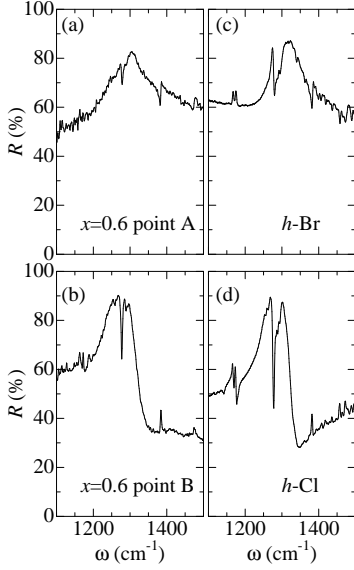


FIG. 2: Reflectance spectra ($E \parallel a$) around 1300 cm^{-1} . (a) and (b) the spectra at the points A and B of $x = 0.6$ sample shown in Fig. 1(d), respectively. (c) and (d) the spectra in κ -(*h*-BEDT-TTF) $_2$ Cu[N(CN) $_2$]Br and κ -(*h*-BEDT-TTF) $_2$ Cu[N(CN) $_2$]Cl, which have been measured in wider area by using the laboratory light source¹⁹.

the dominant metallic background in the $x = 0.5$ sample. Such insulating domains have a tendency to grow with increasing x . In the $x = 0.8$ sample, the insulating region becomes dominant and the metallic domains are found to be remained.

The molecular vibration spectra of the $\nu_3(a_g)$ mode at the metallic and insulating regions are demonstrated in Fig. 2. The spectra in Figs. 2(a) and 2(b) are obtained at the points A and B in the metallic and insulating regions of the $x = 0.6$ sample as shown in Fig. 1(d). The broad peak at 1300 cm^{-1} observed at the point A in Fig. 2(a) has been assigned to $\nu_3(a_g)$ of κ -(*h*-BEDT-TTF) $_2$ Cu[N(CN) $_2$]Br³³. Sharp dips around 1270 cm^{-1} are the overlapping Fano type antiresonance of the terminal ethylene CH_2 vibration of the hydrated BEDT-TTF molecules. The peak shifts to lower frequency and becomes sharper at the point B, which indicates the insulating feature. Such spectra taken at the points A and B resemble those shown in Figs. 2(c) and 2(d), respectively, which have been obtained in the wider area ($\sim 0.5 \times 0.5 \text{ mm}^2$) of the superconducting κ -(*h*-BEDT-TTF) $_2$ Cu[N(CN) $_2$]Br and AF Mott insulating κ -(*h*-BEDT-TTF) $_2$ Cu[N(CN) $_2$]Cl by using the standard laboratory light source¹⁹. The magnitude of the antiresonance of the CH_2 vibration is reduced in the sample partly substituted by the deuterated BEDT-TTF molecules because the deuterated CD_2 vibration has a lower frequency of about 1040 cm^{-1} ³⁴. Possible chemical inhomogeneity such as segregation of deuterated BEDT-TTF can be excluded by checking the magnitude of the

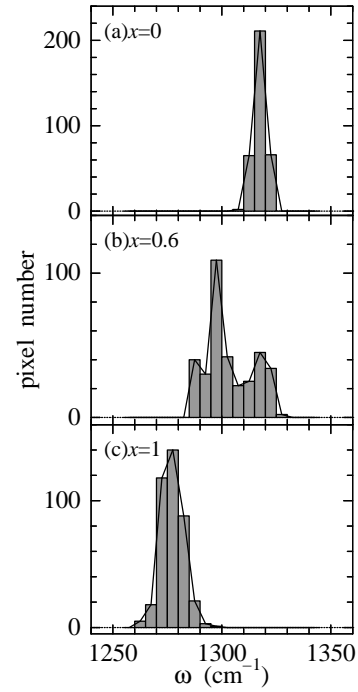


FIG. 3: Pixel number histogram for the $\nu_3(a_g)$ mode frequency ω_3 at 4 K in (a) $x = 0$, (b) $x = 0.6$ and (c) $x = 1$ samples.

antiresonance of the CH_2 vibrations at each scanning point. Therefore the inhomogeneous electronic structure observed by the SMIS measurements has been concluded to be the *electronic phase separation on the macroscopic scale*.

The shape of the metallic and insulating domains is almost circle in case that those domains are small portion of the whole²⁷. On one hand, the configuration of the metal and insulator regions, for example, in the intermediate $x = 0.6$ sample is intricate and no specific size and orientation with respect to the crystal axes are observed. And each region seems not to be located at particular position such as the sample edge, step and scratch of the surface and so on. In addition, these structures and positions of each region are found to be stable to time, which can be confirmed by the mapping time (~ 8 hours / one map) in SMIS measurement.

In order to estimate the metal - insulator volume fraction in the phase separation, the pixel number histograms for ω_3 of $x = 0, 0.6$ and 1 at intervals of 5 cm^{-1} are shown in Fig. 3. In both the end members $x = 0$ and 1 , the histograms show single symmetric narrow peak in Figs. 3(a) and 3(c). In $x = 0.6$, however, ω_3 distributes widely and indicates double peaks. The ratio of the metallic and insulating regions is estimated from the subtotal pixel number of each lower and higher frequency peak.

Figure 4 shows the substitution ratio x dependence of the metallic part ratio deduced from the histogram for ω_3 as shown in Fig. 3. Open circles indicate the results

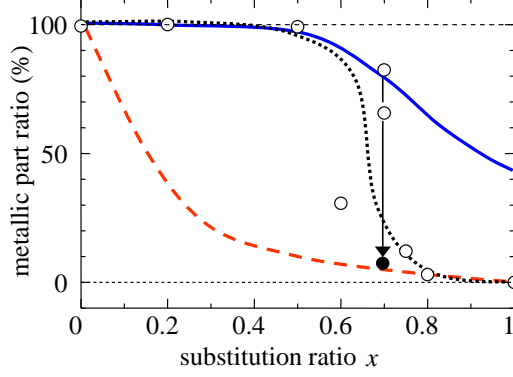


FIG. 4: (Color online) Substitution ratio x dependence of the metallic part ratio of $\kappa\text{--}[(h\text{-ET})_{1-x}(d\text{-ET})_x]_2\text{Cu}[\text{N}(\text{CN})_2]\text{Br}$. Open circles and filled one indicate the results of the slow cooled samples and the quenched $x = 0.7$ No. 2 sample, respectively. Dotted curve is a guide for eyes. Solid and dashed curves represent the superconducting volume fraction deduced from the bulk magnetization measurements²⁸ in the slow cooling and quenched conditions, respectively.

of the slow cooled samples. A filled circle is the result obtained after the quenched cooling process in $x = 0.7$ No. 1 sample. The quenched process will be shown in Fig. 5 in detail. Dotted curve is a guide for eyes. Solid and dashed curves represent the superconducting volume fraction deduced from the bulk magnetization measurements²⁸ in the slow cooling and quenched conditions, respectively. Almost full volume of the metallic nature is kept up to $x \simeq 0.5$ in both the present and magnetization experiments. The metallic part ratio starts to decrease rapidly above $x \simeq 0.5$ and indicates almost fully insulating at $x = 0$ in the present SMIS results. This decrease is rather steeper than the magnetization results. The difference may come from the following two reasons. One is the slight difference of the cooling and sample setting conditions. The cooling speed in the present SMIS experiments is slightly faster than that in the magnetization experiments²⁸. And the sample may be stressed by using carbon paste in the setting to the cold finger, which is different from the stress free setting in the magnetization measurements. These different conditions may affect possible stress and/or strain to the samples, which could modify the band width slightly in the same way as the deuterated BEDT-TTF substitution. Another is the difference of the detecting part of the samples in two experiments. The SMIS results should reflect a part of the surface with a thickness of several μm in depth. Although such μm order thickness is enough for demonstrating the bulk properties, yet the results in the SMIS measurements may overestimate the insulating fraction near the surface.

As mentioned before, the metal-insulator fraction ratio in the phase separation is influenced by the cooling condition in addition to the change with the substitution

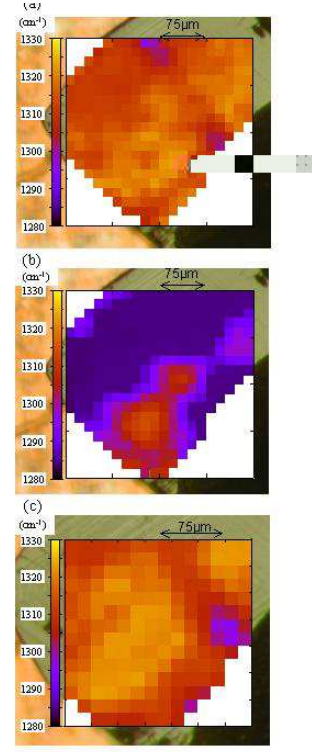


FIG. 5: (Color online) Two dimensional contour map of the peak frequency of the $\nu_3(a_g)$ mode at 4 K in the sample No. 1 of $\kappa\text{--}[(h\text{-ET})_{0.3}(d\text{-ET})_{0.7}]_2\text{Cu}[\text{N}(\text{CN})_2]\text{Br}$; (a) after slow cooling at ~ 0.4 K/min from room temperature to 4 K, (b) after quench at ~ 35 K/min from 120 K to 4 K, and (c) after slow cooling at ~ 1.4 K/min from 100 K to 4 K.

ratio x in principle. Figure 5 shows the variation of the phase separation with the different cooling conditions in the $x = 0.7$ sample No. 1. Each imaging was performed in sequence after the cooling process as follows. First the sample was cooled slowly (~ 0.4 K/min) from room temperature to 4 K (Fig. 5(a)). Second the sample was warmed up to 120 K and then quenched (~ 35 K/min) to 4 K (Fig. 5(b)). Finally the sample was warmed up to 100 K again and then cooled slowly (~ 1.4 K/min) to 4 K (Fig. 5(c)). After the quenched cooling, the insulating fraction drastically increases as shown in Fig. 5(b). The metallic part ratio after such the quenched process is shown in Fig. 4 as the filled circle. The variation between the slow cooled and quenched results is indicated by the vertical arrow. The metallic fraction after the quenched process is consistent with the magnetization experiments²⁸. Such reduced metallic fraction is restored by warming up and cooling slowly again.

The pixel number histogram of ω_3 after slow cooled and quenched process in the $x = 0.7$ sample No. 1 is shown in Fig. 6. Shift to lower frequency side and the formation of the double peak structure of the histogram are found in the results of the quenched state. These variation and reproducibility with the cooling speed and the thermal cycle suggest that the phase separation ob-

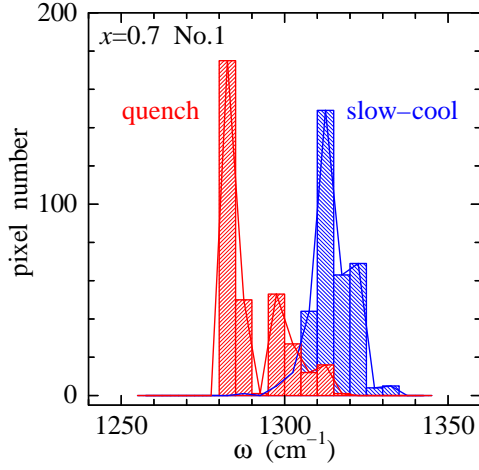


FIG. 6: (Color online) Frequency histogram of the $\nu_3(a_g)$ mode at 4 K after slow cooled and quenched processes corresponding to Figs. 5(a) and 5(b), respectively, in $x = 0.7$ No.1 sample.

served is not attributed to the chemical inhomogeneity such as the segregation of the substituted deuterated BEDT-TTF molecules and extrinsic causes such as the steps, scratches, dislocations on the crystal surface, but closely connected to the Mott first order phase transition in cooperation with the order-disorder glass transition of the terminal ethylene groups of both the hydrated and deuterated BEDT-TTF molecules.

We shall consider the relation between the phase separation observed and the phase diagram near the Mott transition. Figure 7 shows the schematic phase diagram of κ -(BEDT-TTF) $_2$ X. The horizontal axis represents the magnitude of the band width W in comparison to U_{dimer} . The band width increases in right side which corresponds to the weak electron correlation. The materials in κ -(BEDT-TTF) $_2$ X series are indicated at the relative position. The phase separation exists in the narrow $x = 0.5 - 0.8$ region in κ -[(*h*-ET) $_{1-x}$ (*d*-ET) $_x$] $_2$ Cu[N(CN) $_2$]Br. In addition we have confirmed that the phase separation has appeared below T_{cr} in the $x = 0.5$ sample²⁷. Then the Mott transition line should be located around $x = 0.5$ in κ -[(*h*-ET) $_{1-x}$ (*d*-ET) $_x$] $_2$ Cu[N(CN) $_2$]Br. This is in good agreement with the results in the partially deuterated BEDT-TTF molecule based κ -(BEDT-TTF) $_2$ Cu[N(CN) $_2$]Br¹².

The superconductivity in κ -(BEDT-TTF) $_2$ X has been often discussed in comparison with that of the high- T_c copper oxides because of the similarity in appearance of the phase diagram and possible anisotropic *d*-wave pairing symmetry⁹. Then the most of the theoretical investigations have been based on the spin fluctuation mediated anisotropic superconductivity^{35,36,37,38,39,40}. In this line the multicritical phenomenon of the superconductivity and AF insulator has been discussed on the basis of the SO(5) symmetry between two states^{41,42}. From the present experimental points of view, however, the do-

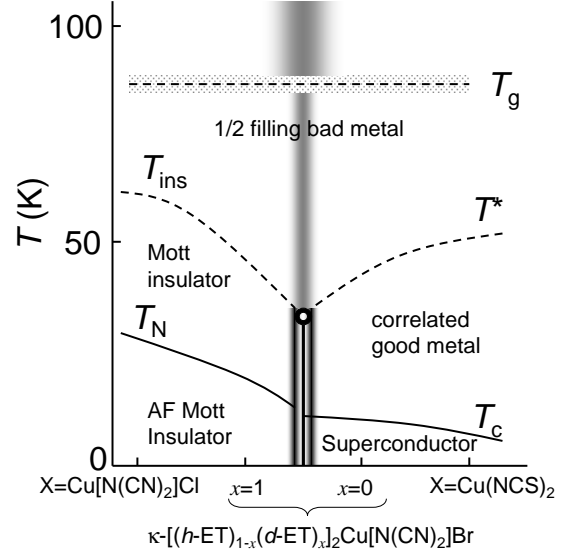


FIG. 7: Schematic phase diagram of κ -(BEDT-TTF) $_2$ X. Open circle indicates the critical end point of the Mott first order transition (vertical solid line). Horizontal axis represents magnitude of the band width in comparison to U_{dimer} . Broad shaded region reflects the possible distribution of the band width due to the terminal ethylene disorder of BEDT-TTF molecules. The width of the distribution is largely overdrawn.

mains consisting of the Mott insulator at $T_N < T < T_{\text{ins}}$ and the correlated good metal at $T_c < T < T^*$ in the phase separation become the AF Mott insulator and superconductor domains independently below T_N and T_c , respectively, without changing any one of those structure, fraction and position. This demonstrates less communication between the superconductivity and AF Mott insulator separated by the first order transition extended up to $T_{\text{cr}} > T_N$ and T_c . It is worth noting here that a model⁴³ of the small-*q* phonon mediated superconductivity has reproduced also the anisotropic *d*-wave gap experimentally observed in κ -(BEDT-TTF) $_2$ Cu(NCS) $_2$ ^{44,45}.

The conformational order-disorder glass transition of the terminal ethylene groups in BEDT-TTF molecules must be important for considering the phase separation because of the large influence of the observed cooling condition dependence. The Mott transition in κ -(BEDT-TTF) $_2$ X is considered to be the band width control type in comparison to the filling control one in the transition metal perovskites such as High- T_c copper oxides. The disorders of the terminal ethylene groups may modulate locally the band width through the local lattice strain. The broad shaded region in the phase diagram represents the distribution of the band width which is schematically overdrawn. The ethylene groups are thermally activating above T_g and should be frozen in the conformational ordered state below T_g ^{20,21}. But some of ethylene groups remain as disorders with different conformation. This re-

mained disorders may induce the local strain of the lattice, resulting in the local modulation of the band width. When this state meets the critical point, the phase separated domains could grow spatially at the nucleation points which are the potential minima for the metal and insulator. It is noted, however, that the disorders do not induce the insulating domains by themselves because amount of disorders must be a few % of the BEDT-TTF molecules at most in slow cooling²² and 5 – 20 % even in the quenched cooling^{20,21}. Then the bistability of two phases near the Mott critical point may be essential for self-assembled metal-insulator domains and the disorders may have the side role as the nucleation.

Similar phase separation on micrometer scale has been found in the current driven low resistive state of the quasi one dimensional organic Mott insulator K-TCNQ⁴⁶. In the low resistive state a visible stripe pattern composed of alternating dark and bright regions emerged with a spacing of 3 to 14 μm . The dark and bright regions could be viewed as the periodic phase segregation into carrier-rich (nondimerized) and -poor (dimerized) regions. Although the pattern formation on micrometer scale is realized in a non-equilibrium state, yet the current-induced coexistence of such the phase segregation has been concluded to be inherent to the correlated electron system where the hypothetical metallic state is adjacent to the Mott insulator.

It is arguable that such metallic domains observed in the present and also the current driven phase separation is stable against the Coulomb interaction between metallic domains. We have no definite information to discuss this problem at present. It must be important to know the dielectric response in the Mott insulator state because the large enough dielectric constant could effectively screen the Coulomb interaction.

IV. CONCLUSION

In conclusion, the experimental evidence of the electronic phase separation is obtained by using the

real space imaging technique on the single crystal surface of the organic Mott system $\kappa\text{-}[(h\text{-ET})_{1-x}(d\text{-ET})_x]_2\text{Cu}[\text{N}(\text{CN})_2]\text{Br}$. SMIS measurements using SR enable us to show the macroscopic size of the domain structure of the insulating and metallic regions. This finding does not exclude the possibility of the nano-scale inhomogeneity inside each domains or each scanning spot because the obtained spectrum may result in the average of nano-scale inhomogeneity in the measured spot. But close agreement between the magnetization and present results suggests that the phase separation occurs on macroscopic scale. The observation of the micrometer scale phase separation is different from the recent findings of the nano-scale electronic inhomogeneity in the strongly correlated inorganic system. The origin of the phase separation may be the combination of the strong electronic correlation near the Mott transition and the characteristic structural disorder inside the BEDT-TTF molecules. In order to make it clear that the mechanism of the phase separation and the process of the domain formation, space imaging technique with the molecular resolution must be developed.

Acknowledgments

We are grateful to T. Moriwaki, T. Hirono and T. Kawase for their technical supports of SMIS measurements at SPring-8. SR experiments were performed at SPring-8 with the approval of JASRI (2003B0114-NSb-np and 2004A0023-NSa-np). This work was partly supported by a Grant-in-Aid for Scientific Research (C) (Grant No. 15540329) from JSPS and Scientific Research on Priority Areas (Grant No. 1603824) from MEXT.

-
- ¹ K. M. Lang, V. Madhavan, J. E. Hoffman, E. W. Hudson, H. Eisaki, S. Uchida, and J. C. Davis, *Nature (London)* **415**, 412 (2002).
 - ² J. M. Tranquada, B. J. Sternlieb, J. D. Axe, Y. Nakamura, and S. Uchida, *Nature (London)* **375**, 561 (1995).
 - ³ M. F  th, S. Freisem, A. A. Menovsky, Y. Tomioka, J. Aarts, and J. A. Mydosh, *Science* **285**, 1540 (1999).
 - ⁴ T. Hanaguri, C. Lupien, Y. Kohsaka, D. -H. Lee, M. Azuma, M. Takano, H. Takagi, and J. C. Davis, *Nature (London)* **430**, 1001 (2004).
 - ⁵ Y. Kohsaka, K. Iwaya, T. Hanaguri, M. Azuma, M. Takano, and H. Takagi, *Phys. Rev. Lett.* (in press), cond-mat/0406089.
 - ⁶ M. Lang and J. M  ller, in *The Physics of Superconductors*, edited by K. H. Bennemann and J. B. Ketterson

- (Springer-Verlag, Berlin 2003), Vol. II.
- ⁷ K. Kanoda, *Hyperfine Interact.* **104**, 235 (1997).
- ⁸ H. Kino and H. Fukuyama, *J. Phys. Soc. Jpn.* **65**, 2158 (1996).
- ⁹ R. McKenzie, *Science* **278**, 820 (1997).
- ¹⁰ S. Lefebvre, P. Wzietek, S. Brown, C. Bourbonnais, D. J  rome, C. M  zi  re, M. Fourmigu  , and P. Batail, *Phys. Rev. Lett.* **85**, 5420 (2000).
- ¹¹ H. Ito, T. Ishiguro, M. Kubota, and G. Saito, *J. Phys. Soc. Jpn.* **65**, 2987 (1996).
- ¹² A. Kawamoto, H. Taniguchi, and K. Kanoda, *J. Am. Chem. Soc.* **120**, 10984 (1998).
- ¹³ Y. V. Sushko, K. Andres, N. D. Kusch, and E. B. Yagbuskii, *Solid State Commun.* **87**, 589 (1993).
- ¹⁴ R. McKenzie, *Comments Condens. Matter Phys.* **18**, 309

- (1998).
- ¹⁵ D. Fournier, M. Poirier, M. Castonguay, and K. Truong, Phys. Rev. Lett. **90**, 127002 (2003).
 - ¹⁶ P. Limelette, P. Wzietek, S. Florens, A. Georges, T. A. Costi, C. Pasquier, D. Jérôme, C. Mézière, and P. Batail, Phys. Rev. Lett. **91**, 016401 (2003).
 - ¹⁷ F. Kagawa, T. Itou, K. Miyagawa, and K. Kanoda, Phys. Rev. B **69**, 064511 (2004).
 - ¹⁸ T. Sasaki, N. Yoneyama, A. Matsuyama, and N. Kobayashi, Phys. Rev. B **65**, 060505 (2002).
 - ¹⁹ T. Sasaki, I. Ito, N. Yoneyama, N. Kobayashi, N. Hanasaki, H. Tajima, T. Ito, and Y. Iwasa, Phys. Rev. B **69**, 064508 (2004).
 - ²⁰ J. Müller, M. Lang, F. Steglich, J. A. Schlueter, A. M. Kini, and T. Sasaki, Phys. Rev. B **65**, 144521 (2002).
 - ²¹ H. Akutsu, K. Saito, M. Sorai, Phys. Rev. B **61**, 4346 (2000).
 - ²² N. Yoneyama, T. Sasaki, T. Nishizaki, and N. Kobayashi, J. Phys. Soc. Jpn. **73**, 184 (2004).
 - ²³ N. Yoneyama, A. Higashihara, T. Sasaki, T. Nojima, and N. Kobayashi, J. Phys. Soc. Jpn. **73**, 1290 (2004).
 - ²⁴ H. Taniguchi, A. Kawamoto, and K. Kanoda, Phys. Rev. B **59**, 8424 (1999).
 - ²⁵ K. Miyagawa, A. Kawamoto, and K. Kanoda, Phys. Rev. Lett. **89**, 017003 (2002).
 - ²⁶ H. Taniguchi, K. Kanoda, and A. Kawamoto, Phys. Rev. B **67**, 014510 (2003).
 - ²⁷ T. Sasaki, N. Yoneyama, N. Kobayashi, Y. Ikemoto, and H. Kimura, Phys. Rev. Lett. **92**, 227001 (2004).
 - ²⁸ N. Yoneyama, T. Sasaki, and N. Kobayashi, J. Phys. Soc. Jpn. **73**, 1434 (2004).
 - ²⁹ S. Kimura, T. Nanba, T. Sada, M. Okuno, M. Matsunami, K. Shinoda, H. Kimura, T. Moriwaki, M. Yamagata, Y. Kondo, Y. Yoshimatsu, T. Takahashi, K. Fukui, T. Kawamoto, and T. Ishikawa, Nucl. Inst. Meth. A **467-468**, 893 (2001).
 - ³⁰ Y. Ikemoto, T. Moriwaki, T. Hirono, S. Kimura, K. Shinoda, M. Matsunami, N. Nagai, N. Nanba, K. Kobayashi, and H. Kimura, Infrared Phys. Techn. **45**, 369 (2004).
 - ³¹ C. S. Jacobsen, *Semiconductors and semimetals* vol. 27, ed. E. Conwell (Academic Press, Inc. New York, 1988).
 - ³² M. J. Rice, Solid State Commun. **31**, 93 (1979).
 - ³³ J. E. Eldridge, K. Kornelsen, H. H. Wang, J. M. Williams, A. V. S. Crouch, and D. M. Watkins, Solid State Commun. **79**, 583 (1991).
 - ³⁴ J. E. Eldridge, C. C. Homes, J. M. Williams, A. M. Kini, and H. H. Wang, Spectrochimica Acta. **51A**, 947 (1995).
 - ³⁵ H. Kino and H. Kontani, J. Phys. Soc. Jpn. **67**, 3691 (1998).
 - ³⁶ H. Kondo and T. Moriya, J. Phys. Soc. Jpn. **67**, 3695 (1998); J. Phys.: Condens. Matter **11**, L363 (1999).
 - ³⁷ K. Kuroki and H. Aoki, Phys. Rev. B **60**, 3060 (1999).
 - ³⁸ J. Schmalian, Phys. Rev. Lett. **81**, 4232 (1998).
 - ³⁹ R. Louati, S. Charfi-Kaddour, A. Ben Ali, R. Bennaceur, and M. Héritier, Phys. Rev. B **62**, 5957 (2000).
 - ⁴⁰ K. Kuroki, T. Kimura, R. Arita, Y. Tanaka and Y. Matsuda, Phys. Rev. B **65**, 100516 (2002).
 - ⁴¹ S. Murakami and N. Nagaosa, J. Phys. Soc. Jpn. **69**, 2395 (2000).
 - ⁴² S. Onoda and N. Nagaosa, J. Phys. Soc. Jpn. **72**, 2445 (2003).
 - ⁴³ G. Varelogiannis, Phys. Rev. Lett. **88**, 117005 (2002).
 - ⁴⁴ K. Izawa, H. Yamaguchi, T. Sasaki and, Y. Matsuda, Phys. Rev. Lett. **88**, 027002 (2002).
 - ⁴⁵ T. Arai, K. Ichimura, K. Nomura, S. Takasaki, J. Yamada, S. Nakatsuji, and H. Anzai, Phys. Rev. B **63**, 104518 (2001).
 - ⁴⁶ R. Kumai, Y. Okimoto, and Y. Tokura, Science **284**, 1645 (1999).